

Contents lists available at **CEPM**

Computational Engineering and Physical Modeling

Journal homepage: [www.jcepm.com](http://www.jcepm.com)

# Aerodynamic Analysis of Autonomous Battery Electric Truck Concepts for Drag Reduction

**Kameel Anirood, Ali Rugbani\***

Department of Mechanical and Mechatronic Engineering, Cape Peninsula University of Technology, Cape Town, South Africa

Corresponding author: [rugbania@cput.ac.za](mailto:rugbania@cput.ac.za)

<https://doi.org/10.22115/CEPM.2022.352845.1217>

## ARTICLE INFO

### Article history:

Received: 22 July 2022

Revised: 29 October 2022

Accepted: 29 October 2022

### Keywords:

Autonomous truck;  
CFD analysis;  
Driverless truck;  
Long haul BET;  
Zero-emission truck.

## ABSTRACT

This research presents an aerodynamic drag analysis of an autonomous battery electric truck (BET) by means of using computational fluid dynamics (CFD) as a simulation tool. The CFD simulation utilises the Reynolds-averaged Navier–Stokes (RANS) equations with a realizable  $k-\varepsilon$  turbulence model and non-equilibrium wall functions to model the near-wall region of the domain. The simulation accuracy is validated against empirical results for the aerodynamic drag on the generic conventional model (GCM) truck, as tested in a wind tunnel. It was found that the overall aerodynamic drag of the vehicle could be reduced by approximately 35.5% without reducing the truck's trailer loading volume. This work demonstrates that autonomous BETs can significantly reduce the overall aerodynamic drag of a truck, thereby reducing energy consumption and greenhouse gas (GHG) emissions for the land freight sector.

## 1. Introduction

In the land freight industry, heavy trucks are a major contributor to greenhouse gas emissions. For trucks travelling at average highway speeds, aerodynamic drag represents 65% of the opposing force that the truck's diesel engine must overcome [1]. This energy utilisation inefficiency contributes greatly towards increasing the emission of greenhouse gases, as well as increasing fuel costs for the trucking company. In moving towards the future goals of a zero-emission truck, battery electric drivetrains represent a favourable future technology path. This push towards an

How to cite this article: Anirood K, Rugbani A. Aerodynamic analysis of autonomous battery electric truck concepts for drag reduction. *Comput Eng Phys Model* 2022;5(2):71–90. <https://doi.org/10.22115/cepm.2022.352845.1217>

2588-6959/ © 2022 The Authors. Published by Pouyan Press.

This is an open access article under the CC BY license (<http://creativecommons.org/licenses/by/4.0/>).



electric future is running parallel with the rapid advancement in autonomous driving technology. This provides the scope for investigating concepts of a driverless BET with the ultimate end goal of optimising the truck-trailer exterior geometry for the purpose of aerodynamic drag reduction. Aside from the potential geometrical and topological layout improvements of an autonomous BET, an autonomous driving mode is potentially smoother, more consistent, more efficient and safer than a human driver. The long term economics of cost of ownership for autonomous BETs is also lower than for conventional diesel internal combustion engine (ICE) trucks [2].

## 2. Literature review

The global transport industry is a trillion-dollar business, which is expected to continue growing in the coming decades. In the Americas, Europe and Nordic countries the transport industry is so large, that it is the leading source of GHGs, and therefore the largest contributor to global climate change for these regions [3]. Road freight in Europe and Nordic countries account for 90% of the total GHG emissions, and heavy-duty vehicles, like large trucks account for 25% of this figure. The usage of heavy-duty trucks within the transport industry is expected to increase in the coming decades [4]. What is more, should business continue as is, heavy trucks are projected to represent over 60% of the total freight activity, and account for over 75% of the lifecycle CO<sub>2</sub> emissions in the transportation industry [5]. A significant amount of research has been done on investigating drag reduction devices that can be fitted to existing ICE heavy-duty trucks [6–16]. Work has also been done on ground-up design improvements for the purpose of aerodynamic drag reduction. While these improvements have been commercialised for decades and ancillary options are available to fleet owners, the current trajectory of GHG emissions for the truck-dominated land freight sector does not meet the long term goals of successfully tackling climate change. With the low fuel efficiency and high GHG emissions, truck design for the future needs to be more energy efficient and less polluting [14]. Goals set out by governments with a focus on future GHG emissions, require a reduction of emissions by 80% to 95% by 2050, in comparison with 1990 GHG emission percentages. A more immediate goal is a reduction in emission levels by 40% by 2030, compared to the emission levels in 1990 [17]. To meet the year 2050 goal, heavy trucks used in the land freight industry will need to become zero-emission vehicles by 2050 [5,18]. Studies have found that in order to meet the goals of a zero-emission truck, direct electric drivetrains are the most energy efficient solution [5,18]. In recent years, the development of Battery Electric Vehicles (BEV) and autonomous vehicles (AV) has seen rapid growth in the passenger car market. The benefits in safety, fuel efficiency, and global GHG emissions that autonomous BEVs exhibit, have seen this technology being adopted by the transportation industry at a rapid rate [19]. In 2016, according to the Global Status Report, the annual road traffic deaths were 1.35 million [20]. In the European Union, 90% of the fatalities were directly caused by human error [21]. In South Africa, this figure was 80% for the year 2015 [22]. In the USA, this figure was 94% in the year 2015 [23]. With the high percentage of accidents caused by human error during driving, the global vehicle market has invested heavily in autonomous technology that would improve safety by allocating the decision-making process to the on-board computer [24]. Apart from the aspects of safety, autonomous BETs also provide a possible aerodynamic and energy utilisation benefit. Without the incorporation of a human driver in the design process, the truck exterior design can be more

aerodynamically streamlined than it currently is. An autonomous driving mode also has the potential of being more linear and less erratic than the driving profile of a human driver.

### 3. Methodology

#### 3.1. CAD models and component selection

The GCM was modelled in Siemens NX software, based on existing geometrical data. The geometrical topology for the autonomous BET components were based on the available literature [25]. The individual component requirements for the demands of a long-haul heavy duty truck were also extracted from the available literature [26]. Verbruggen et al. have also found the optimal peak power required by the electric motors of a heavy-duty truck to be approximately 410kW [26]. Mareev et al. have found this figure to be 376kW. For the purposes of this research the figure of 410kW was used for the electric motor system peak power requirement [27]. In terms of the type of electric motor which best suits the requirements of a long-haul BET, the PMSM type has been found to be optimal [26,28,29]. Verbruggen et al. have also found that for heavy-duty electric trucks, the optimal battery size falls into the range 221kWh to 210kWh. The figure of 221kWh was used for the battery energy requirement [26]. Unlike conventional ICE trucks which normally have 18 speed transmissions, BETs make use of just two to four speeds. Autonomous systems are not the major components in terms of physical size compared to those described above. For this reason, component selection was not done for the autonomous system. With the requirements of the individual components defined, research was done in finding currently available commercial solutions for each component.

#### 3.2. Generic conventional model GCM

The model used to validate the CFD setup and accuracy is the GCM. This is a simplified geometry used to represent a modern tractor-trailer model. The underbody of the tractor and the trailer in the GCM has been simplified and approximated by flat surfaces [30]. Based on experiments done by Satran, the drag coefficient measured at a yaw angle of zero degrees was measured to be 0.397 [31]. This experiment did not use a rolling road. The GCM and its basic dimensions can be seen in Figure 1 below

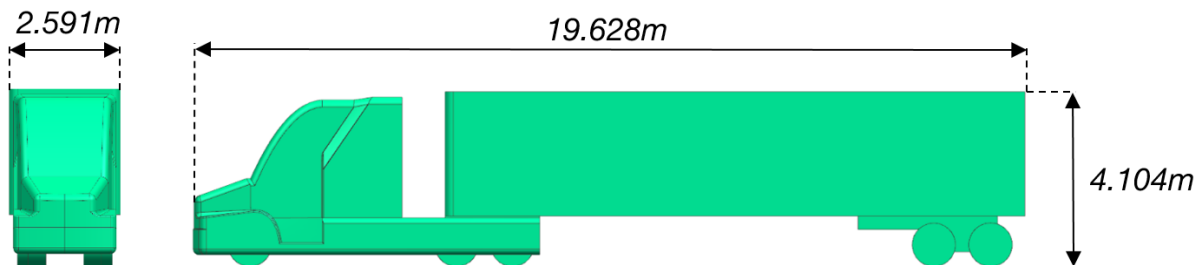


**Fig. 1.** Basic dimensions of the GCM.

#### 3.3. Computational domain

In terms of the size of the computational domain and the positioning of the GCM within the domain, Lanfrit recommends that the domain should extend three vehicle lengths in front of the

GCM, and five vehicle lengths behind the GCM. Lanfrit also recommends that the GCM not displace more than 1.5% of the total cross-sectional area [32]. With these parameters taken into account, the CFD computational domain is shown in Figure 2 below. The GCM is a symmetrical model, and as such, the domain was symmetrical along the GCM longitudinal axis. This had the benefit of reducing the computational power demand and time by half. The available computing power limits the scope of this research to only consider flows without yaw.

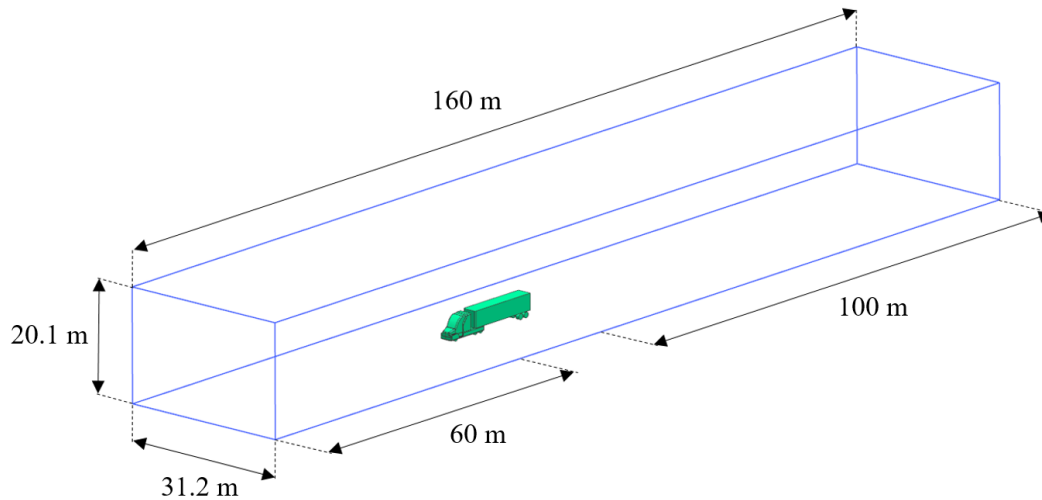


**Fig. 2.** CFD computational domain.

### 3.4. Boundary condition

For the purposes of the validation model, the floor of the domain was simulated as a stationary wall. The floor was simulated as a rolling road for all simulations after the validation. The floor is simulated to move in the direction and at the same speed as the incoming air flow. The face of the domain where the air flow enters, was modelled as a velocity inlet. The properties of the incoming flow, such as the speed magnitude, airflow direction and turbulence were specified at this velocity inlet plane. The domain exit was modelled as a pressure outlet, with a pressure equal to atmospheric pressure. The longitudinal symmetry plane was modelled with a symmetry boundary condition with zero shear stress. The GCM was modelled as a stationary wall with a no-slip shear condition.

### 3.5. Mesh generation and accuracy

The mesh was first created in Ansys Fluent as a tetrahedron element mesh. This was later converted to a polyhedral based mesh since the computational time is greatly reduced without any great losses in accuracy when using a polyhedral mesh. A refinement box was added to the mesh model to provide a more detail rich mesh in the areas of aerodynamic interest. The mesh and the refinement box can be seen in Figure 3 below.

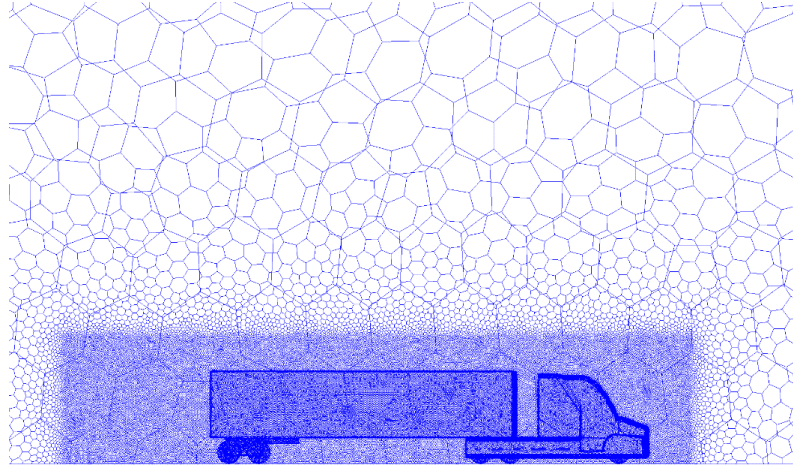


**Fig. 3.** Mesh refinement box around the GCM.

One of the key attributes that define mesh quality is the dimensionless distance from the wall ( $Y^+$ ). When solving the viscous sub-layer of the boundary layer, a  $Y^+$  value of approximately  $< Y^+ < 500$  is acceptable [33]. The wall function approach is suitable to many bluff bodies as well as modern vehicle design [34]. Within the inflation layer of prism cells generated from the surface mesh, the height of the first prism cell ( $\Delta y_1$ ) within this inflation layer is important to achieving an adequate  $Y^+$  value. To determine the required  $\Delta y_1$ , the Reynolds number for the GCM had to be determined. The equation for finding the Reynolds number is given by equation (1) below [35].

$$Re = \frac{\rho UL}{\mu} \quad (1)$$

Where  $\rho$  is the fluid density,  $U$  is the freestream velocity,  $L$  is the characteristic length, and  $\mu$  is the fluid viscosity. For simulations of the GCM:  $\rho = 1.225 \text{ kg/m}^3$ ,  $U = 27.8 \text{ m/s}$ ,  $\mu = 1.79 \times 10^{-5} \text{ kg/m.s}$ , and  $L = 2.267 \text{ m}$ .  $L$  in this case is taken as the width of the frontal area of the GCM that is perpendicular to the incoming flow. When these values are input into equation (1), the value of the Reynolds number is found to be  $4.93 \times 10^6$ . The governing equation for  $\Delta y_1$  is given by equation (2) below [33].

$$\Delta y_1 = \frac{Y^+ \mu}{\rho U_\tau} \quad (2)$$

Where  $U_\tau$  is the fluid frictional velocity that is given by equation (3) below [36].

$$U_\tau = \sqrt{\frac{\tau_w}{\rho}} \quad (3)$$

Where  $\tau_w$  is the wall shear stress, which is given by equation (4) below [37].

$$\tau_w = \frac{1}{2} C_f \rho U^2 \quad (4)$$

Where  $C_f$  is the skin friction coefficient for external flows, given by  $C_f = 0.058 Re^{-0.2}$  [37].

Using a value for  $Y^+$  of 100, and solving equation (2), the value of  $\Delta y_1$  is found to be 4 mm. Thus the height of the first prism cell in the boundary layer is manually set to 4 mm. The equation for the approximation of the boundary layer thickness is given by equation (5) below [34].

$$\delta = \frac{0.37x}{Re^{\frac{1}{5}}} \quad (5)$$

Where  $x$  is the characteristic length. Using the calculated value of  $Re$  and using a value of 2.267 m for the characteristic length  $x$ , the approximate boundary layer thickness is calculated to be 39.5 mm. To define the inflation layer, the first layer height was set to 4 mm, a growth rate for the subsequent layers was set to the default 20%. Sufficient layers were added to cover the calculated boundary layer thickness of 39.5 mm. The inflation layer on the front of the GCM tractor can be seen in Figure 4 below. It can be seen that prism cells merge into the polyhedral cells with relatively little skewness.

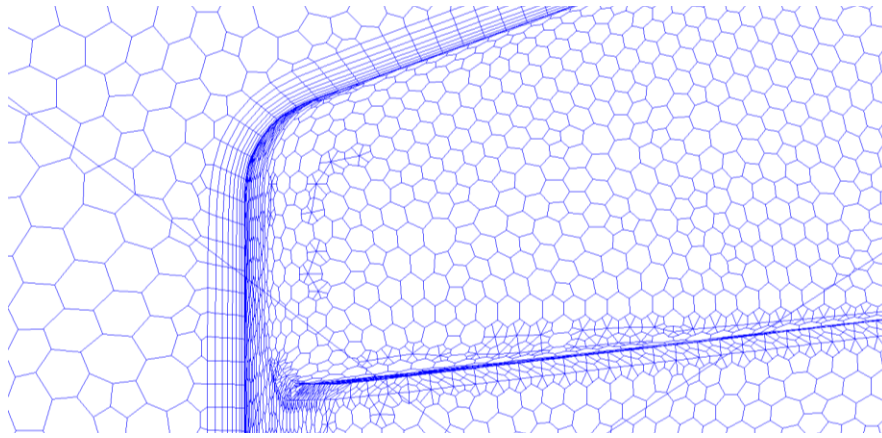


**Fig. 4.** Inflation layer on the GCM.

### 3.6. CFD solver setup

The simulation utilised the RANS equations as this study was concerned with the effect and comparison of multiple geometry changes on drag. The RANS strategy has the advantage of reduced computational time compared to other simulation models. The coupled solver was selected over a segregated solver as it reached a converged result much faster than the segregated solver [38]. The realizable  $k-\varepsilon$  model was selected as the turbulence model. Non-equilibrium wall functions were used to model the near-wall region of the domain as they had the advantage over standard wall functions, in that they account for the effects of pressure gradients, provide more accurate descriptions of flow separation, reattachment, and especially in their ability to accurately predict skin-friction coefficients [38].

### 3.7. Conceptual autonomous BETs

The aerodynamic advantage of an autonomous BET over a conventional ICE truck is that the geometry can be more streamlined. The inclusion of a cabin for the driver, as well as a raised nose to accommodate the ICE and associated systems gives the conventional ICE truck a larger frontal area which dramatically increases aerodynamic drag. Two autonomous concepts were created: Concept One and Concept Two. Concept One was based on a least frontal area approach, which

results in a theoretically lower aerodynamic drag for the tractor. Concept Two was based on approximating the longitudinal geometry of the tractor-trailer combination to resemble that of an aerofoil, again for the purposes of reducing overall aerodynamic drag.

### 3.8. Concept One

The first concept was designed with a minimal frontal area approach, and a design envelope that fits around the auxiliary systems with no extra features exposed to the airflow. This was done as the frontal area of a vehicle is directly proportional to the aerodynamic drag. Unlike the nose of the GCM, the nose on Concept One is devoid of any surfaces that are perpendicular to the airflow which would otherwise greatly increase flow separation and aerodynamic drag. Concept One is shown in Figure 5 below, also shown is the schematic for the autonomous BET

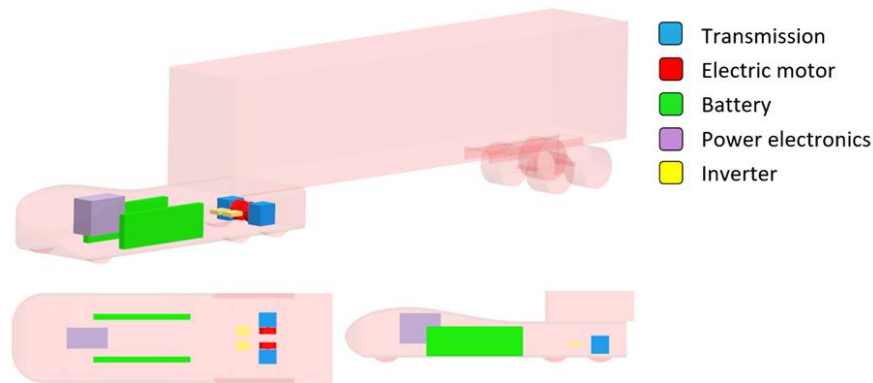


**Fig. 5.** Concept One schematic shown in isometric view (top), plan view (bottom left), and side view (bottom right).

### 3.9. Concept Two

Concept Two smoothly transitions the airflow along the surfaces without many abrupt geometry changes, this was done to reduce flow separation and aerodynamic drag. The tractor-trailer gap was reduced as much as possible since there is a proportional relationship between tractor-trailer gap and aerodynamic drag [10]. The upper most surface of the tractor is 5 mm higher than that of the leading edge of the trailer, this was done to ensure the airflow that transitions from the tractor to the trailer flows over the top of the trailer. Figure 6 below shows the CAD geometry of Concept Two.

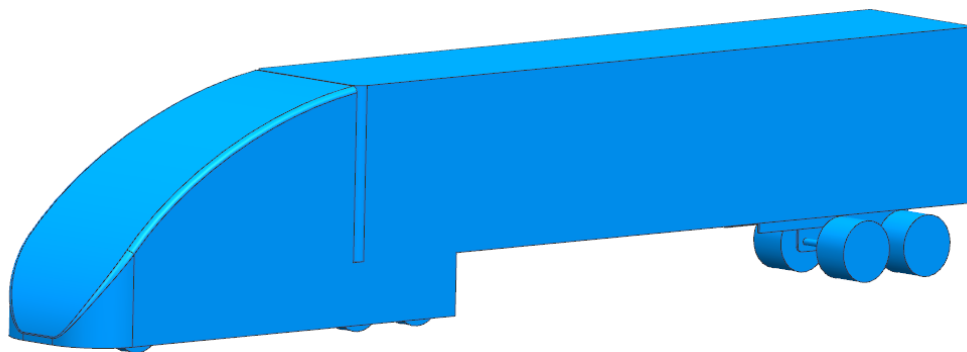


**Fig. 6.** Autonomous BET Concept Two.



### 3.10. Iterative design

The CFD results for the concept autonomous BET was evaluated in terms of aerodynamic drag, pressure coefficient, flow velocity, vorticity, turbulence and wake formation. Areas which appeared to be contributors to increased aerodynamic drag were identified. Geometrical changes were proposed and added to each iteration of the concept based on the CFD results, with the aim of reducing the overall aerodynamic drag as well as reducing the wake size and intensity. This was an iterative process that continued until simple design changes could no longer be made without greatly impacting the practicality of the vehicle to perform its normal logistical function.

## 4. Study results

### 4.1. GCM

Figure 7 below shows the graph for the drag coefficient of the GCM, with convergence after 1232 iterations. The drag coefficient value stabilised to 0.403.

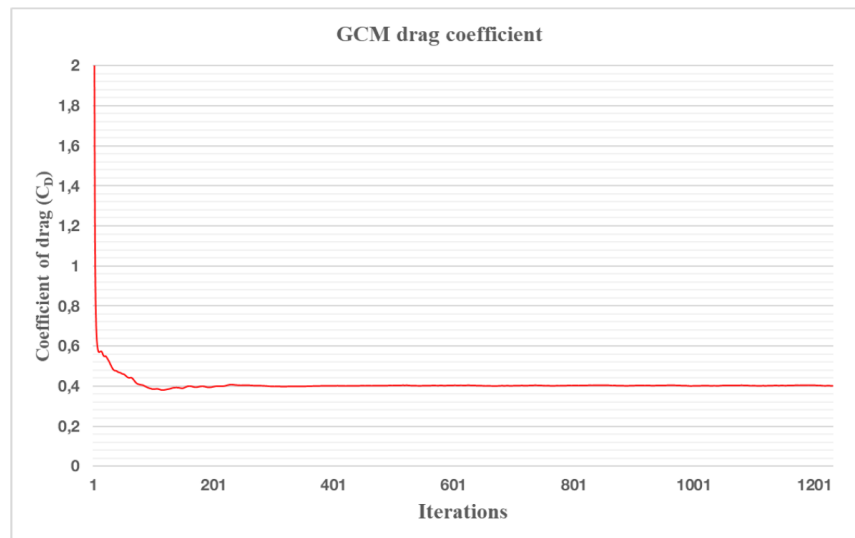


**Fig. 7.** Drag coefficient graph for the GCM.

Compared to the experimental value for  $C_D$  of 0.397 found by [31], the CFD simulation result for  $C_D$  was 1.244% higher. This discrepancy was due to the limitation of element quantities of the student version of Ansys Fluent as well as the computational limits of the solving computer. Examining the pressure distribution over the GCM, as shown in Figure 8, high pressure zones can be seen at the nose, the intersection between the hood and windscreen, as well as in the frontal area of the trailer. Another high pressure zone can be seen in the geometry of the cab door recess, and the step created for easier driver entry into the cabin. Figure 9 shows the flow vorticity magnitude over the GCM, problem areas can be seen in the top of the tractor hood, the trailing edge of the tractor roof, the trailing edge of the tractor floor, and the leading edge of the trailer roof.



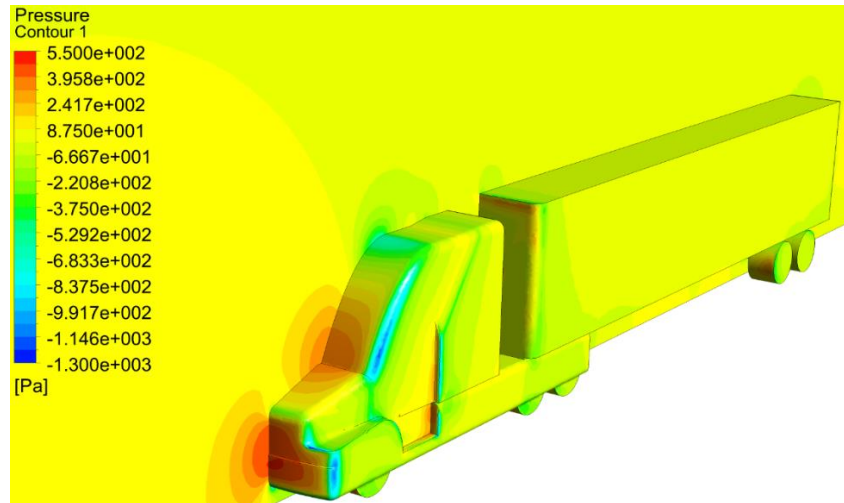


**Fig. 8.** Pressure distribution over the GCM.

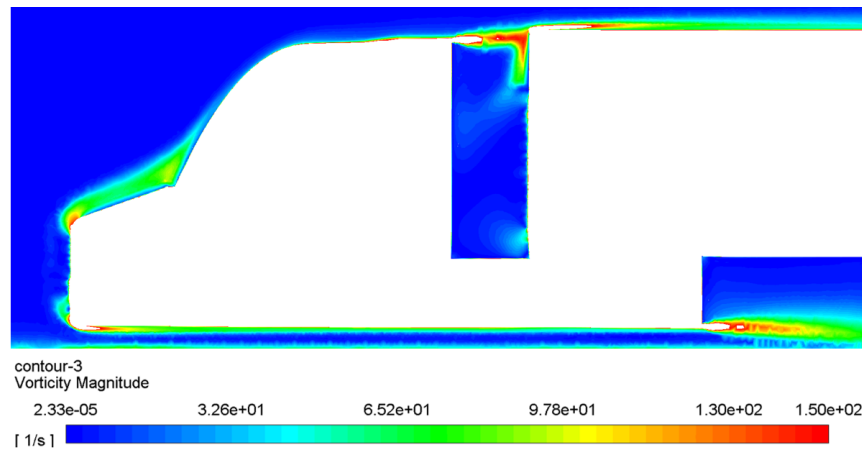


**Fig. 9.** Flow vorticity magnitude over the GCM.

The GCM geometry creates highly turbulent flow on the front face of the trailer. The bluntness of the nose on the GCM as well as on modern trucks is a consequence of legislation on overall length as well as having to accommodate the engine and cooling package/s of a modern diesel ICE into the design. It is evident that there are areas of the GCM which contribute significantly to the overall aerodynamic drag on the vehicle. The most prominent of these areas are the tractor blunt nose, the transition from the hood to the cabin windscreen, the tractor-trailer gap, as well as the transition of the floor of the tractor into the rear face of the tractor.

#### 4.2. Concept One

This concept was simulated under the exact domain specifications as was used in the GCM simulation, but with one major change; this concept as well as the concepts that follow were simulated with a rolling road condition applied to the floor of the CFD domain. The  $C_D$  value for this concept was found to be 0.68. The main reason for this dramatic increase in drag is that the entirety of the trailer front face is exposed to the incoming airflow. This flow separation area proved to be the single greatest area responsible for the aerodynamic drag on the vehicle. Figure 10 shows the flow pressure coefficient over Concept One.

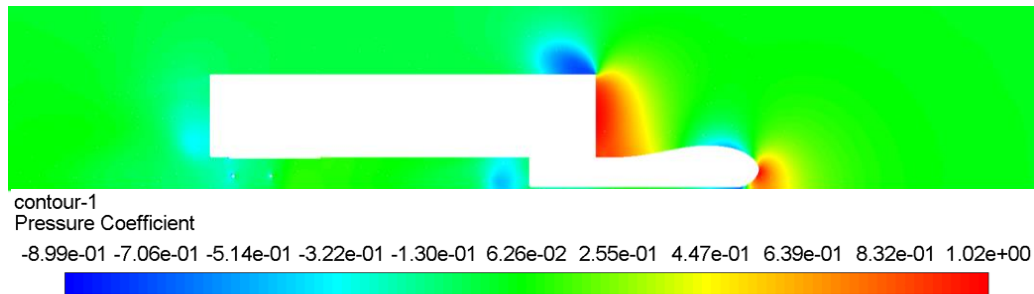


**Fig. 10.** The flow pressure coefficient over Concept One.

It can be seen how the trailer created a very high pressure zone in front, and a low pressure zone on top of the trailer front edge, as the flow separated in this region. The tractor nose also presented a significant pressure rise. To lessen this effect, the nose radius as well as its height above the ground plane was lowered.

#### 4.3. Concept Two

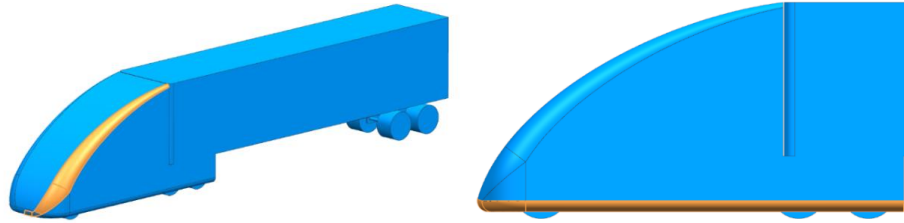
The lessons learned from Concept One were applied to the construction of Concept Two, especially in the area of the tractor nose. Looking at the flow pressure coefficient over Concept Two, as shown by Figure 11 below, it is clear that the high pressure zone at the nose had been reduced compared to Concept One. It was also clear that the transition area from the front of the truck to the sides create a sharp drop in pressure in this area. To reduce this sharp low pressure effect, a larger radius transition was examined in the revision to Concept Two. The lower surface of the truck in Concept Two creates a sharp geometry change which results in flow separation and an increase in vorticity in this area, both of which contribute to increased aerodynamic drag. To reduce this effect, a radius was added to the floor of the truck in subsequent revisions of Concept Two.



**Fig. 11.** Flow pressure coefficient over Concept Two (left), and a magnified view of the frontal area (right).

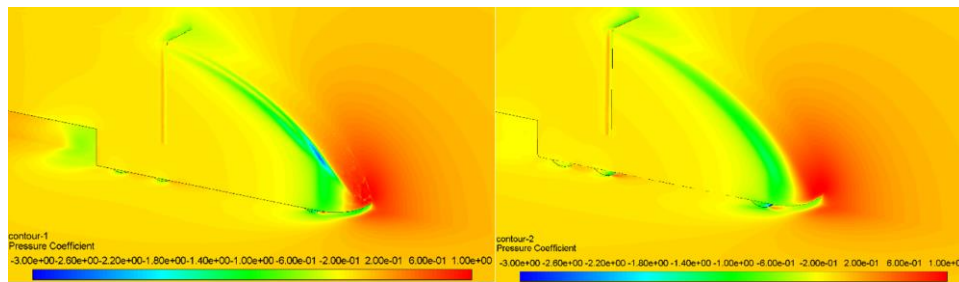
#### 4.5. Concept Two – Revision A

The required geometry changes mentioned above are shown in Figure 12. For the side radius, a non-linear radius was created. A large radius of 500 mm was added at the lower area, while a tighter 80 mm radius was added at the top. The reason for a tighter radius at the top was to avoid an abrupt transition of airflow from the tractor to the top front edge of the trailer. A linear 200 mm radius was added to the tractor floor to reduce the adverse aerodynamic effects.



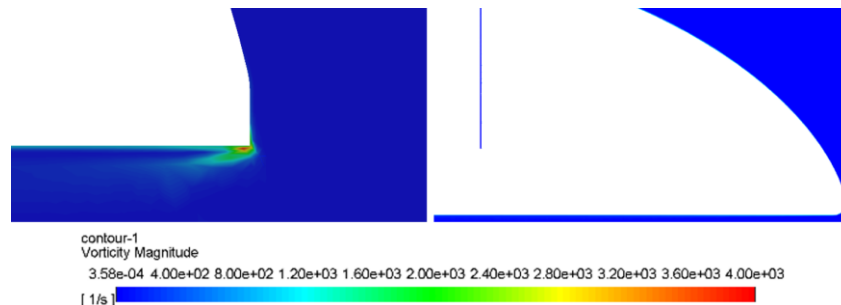
**Fig. 12.** Tractor side (left) and floor (right) radius changes for Concept Two - Revision A, highlighted in orange.

Figure 13 below shows a comparison of the pressure coefficient between Concept Two (left) and Concept Two - Revision A (right). It is clear that the radius changes reduced the sharp pressure drop on the side of the vehicle – the strong blue region (left) has been dispersed evenly across the geometry (right).



**Fig. 13.** Comparison of pressure coefficient between Concept Two baseline (left), and Concept Two - Revision A (right).

Figure 14 shows the dramatic reduction in vorticity at the nose of the truck from Concept Two baseline (left) to Concept Two Revision A (right).



**Fig. 14.** Comparison of vorticity magnitude between Concept Two baseline (left), and Concept Two - Revision A (right).

#### 4.6. Concept Two – Revision B

The next area of interest was to reduce the wake and vorticity at the rear of the trailer. Boat tails have proven to be successful in reducing the wake in this region, and lowering the overall aerodynamic drag of the truck [14]. Hyams et al. have found that boat tail sections which have a 15° angle from the trailer centreline and a length equal to a quarter the width of the trailer have proven to work well in reducing wake formation and size, as well as reducing the aerodynamic drag. This concept is shown in Figure 15 below (boat tail highlighted in grey) [11].

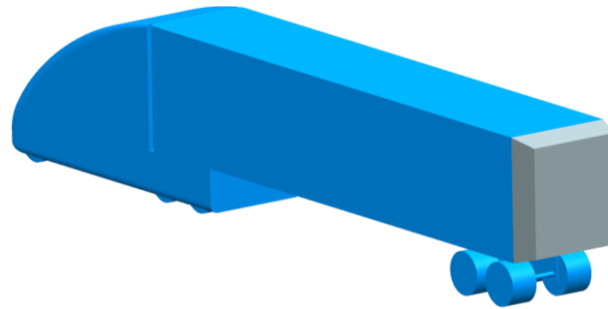


**Fig. 15.** Concept Two – Revision B.

Figure 16 and 17 examine visually the effect of adding a boat tail. The wake size as well as the intensity have been dramatically reduced.

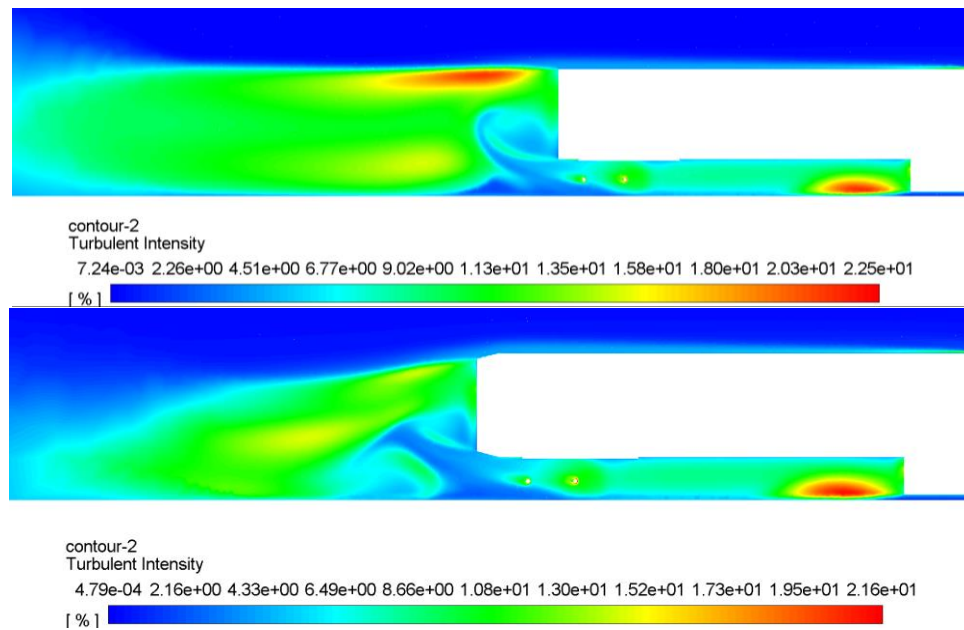


**Fig. 16.** Side view comparison of the turbulent intensity of the flow between Concept Two – Revision A (top), and Concept Two – Revision B (bottom).

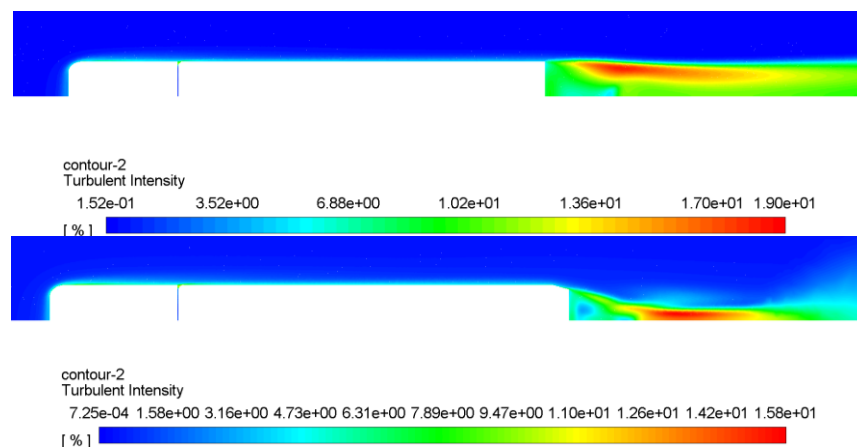


**Fig. 17.** Plan view comparison of the turbulent intensity of the flow between Concept Two – Revision A (top), and Concept Two – Revision B (bottom).

#### 4.7. Concept Two – Revision C

Skirts were the next design feature that was examined. Figure 18 shows the geometry for Concept Two – Revision C (left), and also shows a section of the tractor rear floor that was modified to promote a smoother transition of airflow over the back of the tractor (right). The skirts were not extended beyond the trailer wheels. This was done to maintain the practicality of easily changing a trailer wheel.

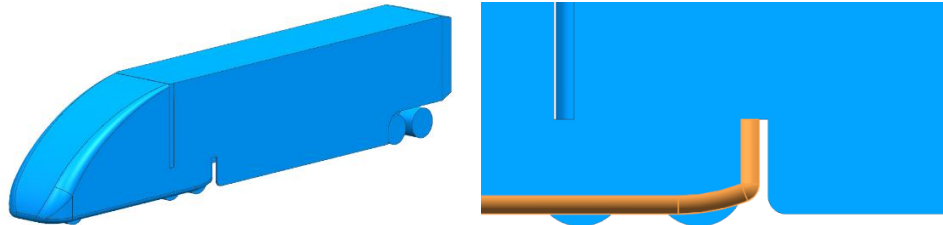


**Fig. 18.** Concept Two – Revision B – full view (left), modified tractor rear (right – highlighted in orange).

Figure 19 shows the reduction in turbulent intensity with Concept Two – Revision C. The gap between the rear of the tractor and the leading edge of the skirts allows for airflow to “leak” into the area under the trailer which causes an increase in turbulence in this area.

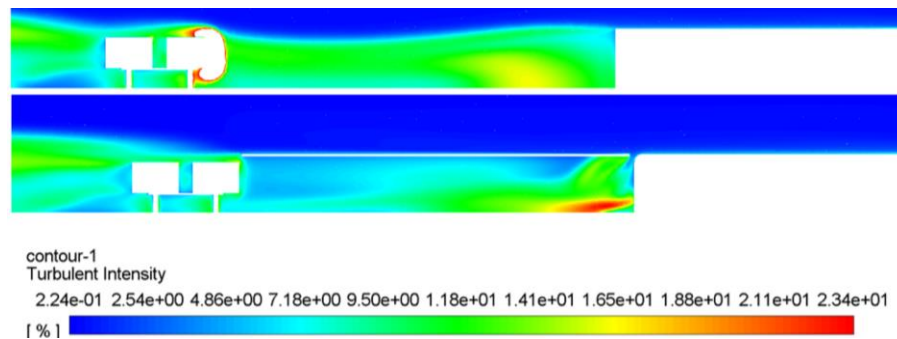


**Fig. 19.** Plan view comparison of the turbulent intensity of the flow between Concept Two – Revision B (top), and Concept Two – Revision C (bottom).

#### 4.8. Concept Two – Revision D








The final design feature examined was a tapered trailer roof. This was to simulate the aerofoil profile as much as possible. A  $1^\circ$  taper of the roofline, measured from the front edge of the trailer roof was added. This modification can be seen in Figure 20 below, highlighted in orange. This was the only concept which negatively impacts the practicality of the tractor-trailer as the total load volume has decreased.



**Fig. 20.** Concept Two – Revision D, removed geometry for the tapered roof feature is highlighted in orange.

The results of  $C_D$  and the change reference to the GCM for all concepts are shown in Table 1.

**Table 1**Comparison of  $C_D$  values for all CFD simulated models.

3D CAD	Model name	$C_D$	% change in $C_D$ relative to GCM
	GCM	0.403	0.00
	Concept One	0.680	+40.70
	Concept Two	0.354	-12.16
	Concept Two – Revision A	0.331	-17.87
	Concept Two – Revision B	0.275	-31.76
	Concept Two – Revision C	0.260	-35.48
	Concept Two – Revision D	0.251	-37.72

A discussion of each simulation result is given below.

GCM – There are obvious areas in the GCM which contribute to increased drag, namely the very blunt nose, the abrupt angle change that is present in the transition of the tractor hood to the windscreen, the driver entry step, the cabin doors and the tractor-trailer gap. These areas also have higher flow vorticity magnitudes, and lower flow velocity magnitudes which result in increased aerodynamic drag.

Concept One – While the tractor for this concept represents the smallest frontal area exposed to airflow of all the models simulated, the frontal area of the tractor-trailer combination is approximately the same as all other models tested. As a result, the front face of the trailer presents a large perpendicular obstacle to the incoming airflow greatly increasing drag. The generated wake for this model is also greater than that of the GCM, due to the flow separation that occurs at the trailer front leading edges disrupting the flow along the length of the trailer.

Concept Two –The smooth transition from nose to the top of the trailer leading edge resulted in the fewest flow separation points compared to the two models discussed above. The transition from nose to floor created a flow separation point as well as a source for increased vorticity, resulting in disrupted flow along the floor of the truck. While the blended geometry that transitions

from upper surface of the tractor to the left and right sides of the tractor was added to reduce the possibility of flow separation, this area also resulted in creating a pressure drop on the blended surface.

Concept Two – Revision A – The transition area was modified with an increased radius transition, as well as adding a curved transition to the floor. The vorticity magnitude at the nose lower surface was reduced by approximately 40% when compared to Concept Two. The addition of the curved floor transition also increased the velocity magnitude under the floor of the tractor by approximately 3%.

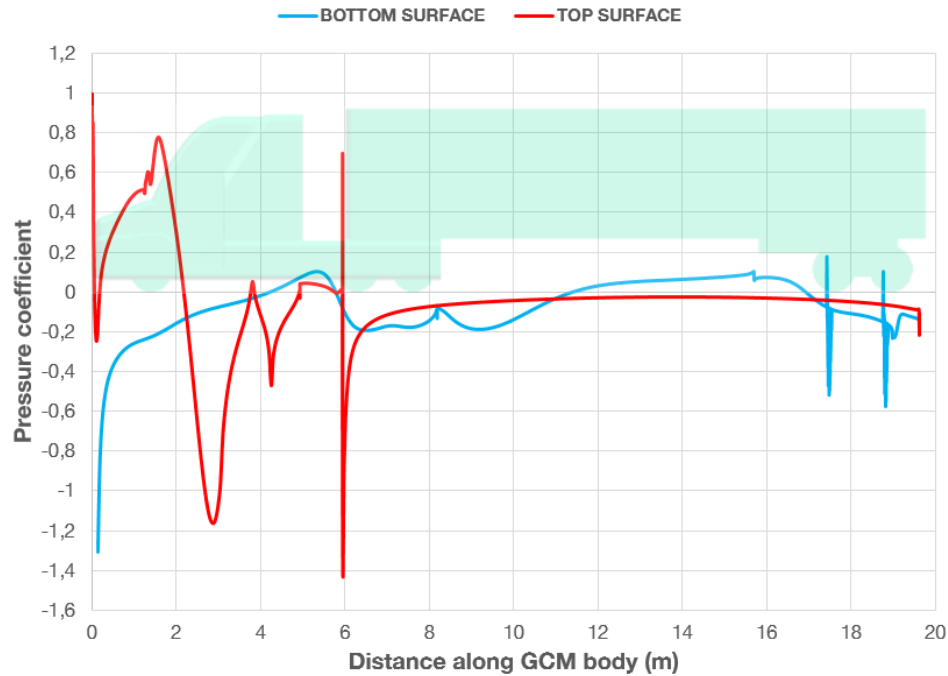
Concept Two – Revision B – Both the wake size and intensity was reduced in the concept when compared to Concept Two – Revision A. In both Concept Two – Revision A and Concept Two – Revision B, there are two vortex flows that occur at the rear of the trailer, one from the top surface of the trailer and one from the lower surface of the trailer. The vortex generated at the top is larger in magnitude than that of the one created at the bottom surface, due to the trailer wheels and axles disrupting the airflow and removing energy from the airflow. With the addition of the boat-tail, the upper vortex turbulent intensity was reduced by approximately 38% when compared to Concept Two – Revision A.

Concept Two – Revision C – Trailer skirts as well as a smoother tractor rear transition were added to this concept. The most significant aspect for adding the trailer skirts was limiting the amount of airflow flowing from the tractor sides to the underside of the trailer, as well as limiting the amount of airflow from the sides of the trailer itself flowing to the underside of the trailer. The skirts resulted in lowering the turbulent intensity caused by the trailer leading wheel by approximately 65% compared to the absence of skirts. The overall turbulent intensity under the trailer was reduced with the addition of the skirts.

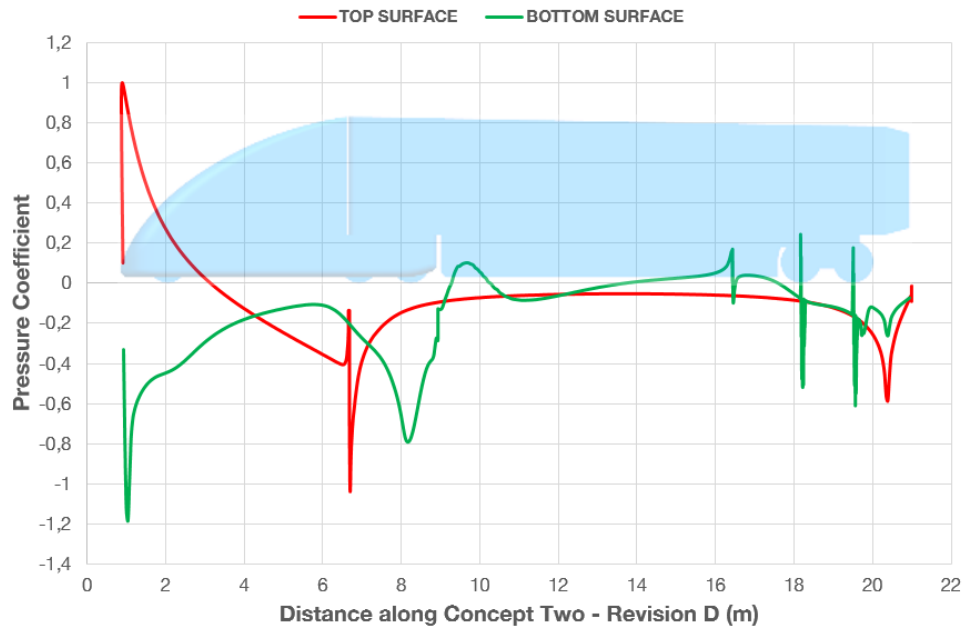
Concept Two – Revision D – The tapered roofline more closely approximates the profile of an aerofoil, which should theoretically provide a reduction in aerodynamic drag. The addition of a taper to the trailer roofline also resulted in reducing the turbulent intensity of the flow by approximately 5% compared to Concept Two – Revision C. The flow vorticity at the top rear of the trailer was reduced by approximately 32% when compared to that of Concept Two – Revision C.

Figure 21 and 22 show the pressure coefficient over the longitudinal centreline section of the GCM and Concept Two – Revision D, respectively. Inspecting the curves for the top surface of each model for the range 0m to 6m, it is clear how much smoother the curve is for Concept Two – Revision D. This is a reflection of fewer flow detachment areas, and lower turbulence for Concept Two – Revision D. Peak high and peak low values are also lower for Concept Two – Revision D. The curves for the bottom surface show similar trends between models, with higher peak values for the Concept Two – Revision D trailer. This is due to the influence of a rolling road, road boundary layer, the sealing effect of the skirts, and higher flow velocity under the Concept Two – Revision D trailer.





**Fig. 21.** Pressure coefficient over the GCM body.



**Fig. 22.** Pressure coefficient over the Concept Two – Revision D body.

Figure 23 and 24 show the airflow turbulent intensity over Concept Two – Revision D and the GCM respectively. It is clear that the size, and particularly the turbulent intensity is greatly reduced in Concept Two – Revision D compared to the GCM. This difference is further emphasised when viewing the plan views of the GCM and Concept Two – Revision D.

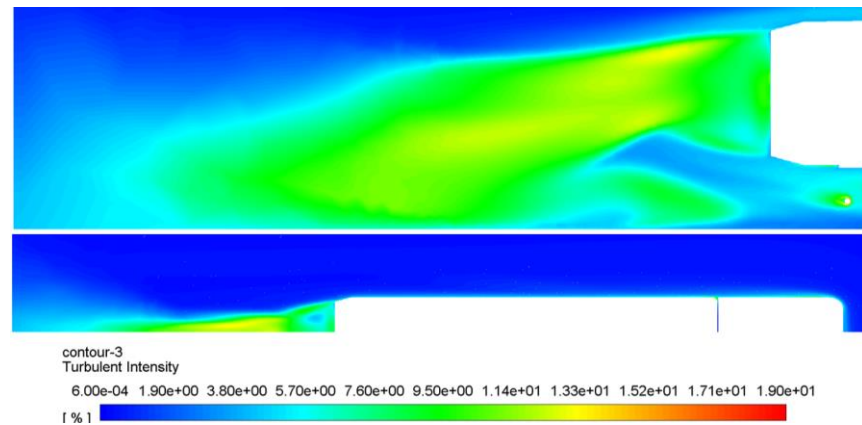


**Fig. 23.** Side view (top) and plan view (bottom) of the airflow turbulent intensity over Concept Two – Revision D.

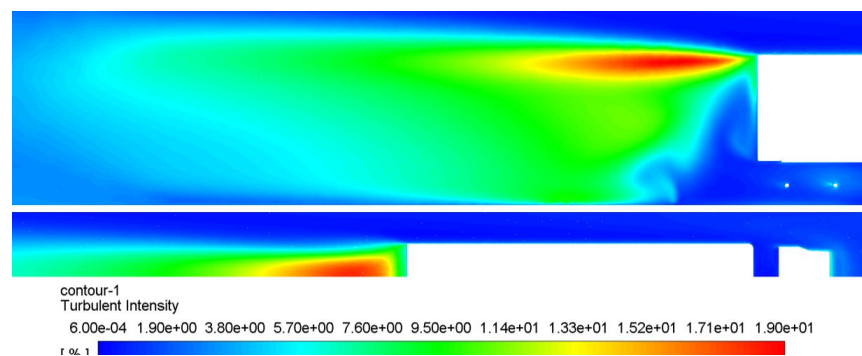


**Fig. 24.** Side view (top) and plan view (bottom) of the airflow turbulent intensity over the GCM.

Figure 25 and 26 show the pressure coefficient over Concept Two – Revision D and the GCM respectively. The multiple high pressure spots on the GCM tractor have been reduced to a single high pressure zone at the front of the Concept Two – Revision D tractor. The GCM high pressure zone between the rear of the tractor and the front of the trailer, as seen in Figure 27, is dramatically reduced in Concept Two – Revision D. The GCM also had a localised high pressure zone under the trailer, whereas the pressure distribution was more evenly dispersed and of a lower magnitude in Concept Two - Revision D.

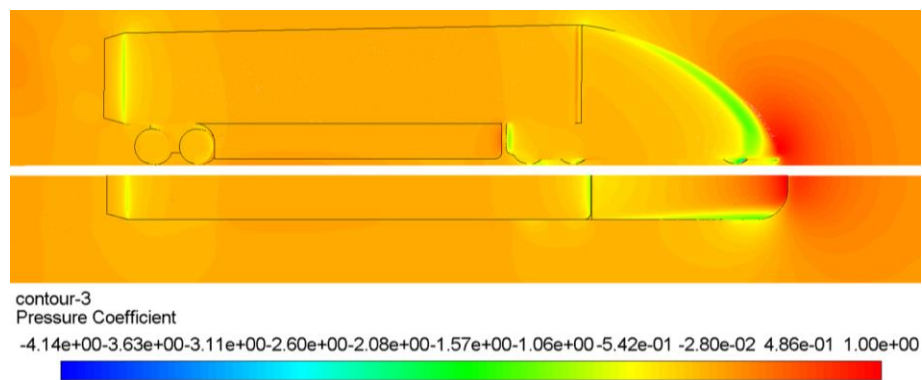


**Fig. 25.** Side view (top) and plan view (bottom) of the airflow pressure coefficient over Concept Two – Revision D.

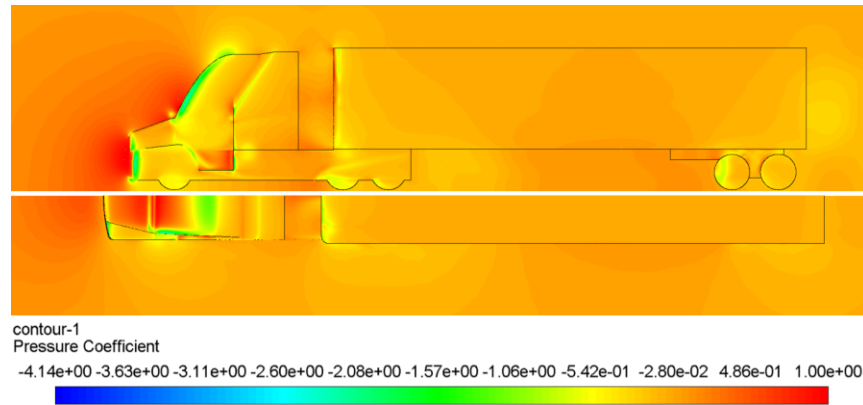


**Fig. 26.** Side view (top) and plan view (bottom) of the airflow pressure coefficient over the GCM.

## 5. Conclusion

The aim of this work has been to determine the possible aerodynamic drag reduction for an autonomous BET. There has been considerable amount of research on large heavy-duty trucks, and on how the aerodynamic drag can be reduced either through ground up design or with the addition of ancillary items. The study found that an approximately 18% reduction in aerodynamic drag can be gained without the truck owner or logistics company having to invest in trailer modifications. With low investment options such as a boat tail and trailer side skirts, a reduction of aerodynamic drag of approximately 32% and 35.5% respectively is possible. In terms of practicality, maintenance and load space, the boat tail and side skirts have no negative effects. A  $C_D$  value of 0.260 can be achieved for an autonomous BET compared to 0.403 for a simplified conventional diesel ICE truck, with no compromise in load practicality for the autonomous BET.

## Declarations

### Availability of data and materials

The datasets generated during the current study are available from the corresponding author on reasonable request.

### Competing interests

The authors declare that they have no competing interests.

### Funding

There was no financial support or sponsors to this research.

### Authors' contributions

The two authors contributed to the planning and preparation of the article. The first author performed the aerodynamic testing, data analysis, and the writing of the paper. The second author read, edited and approved the final manuscript.

## Acknowledgements

Not applicable.

## Ethics

The nature of this research does not raise any ethical concerns.

## References

- [1] McCallen RC, Salari K, Ortega JM, DeChant LJ, Hassan B, Roy CJ, et al. Doe's effort to reduce truck aerodynamic drag - joint experiments and computations lead to smart design. 34th AIAA Fluid Dyn. Conf. Exhib., 2004. <https://doi.org/10.2514/6.2004-2249>.
- [2] Sanguesa JA, Torres-Sanz V, Garrido P, Martinez FJ, Marquez-Barja JM. A Review on Electric Vehicles: Technologies and Challenges. *Smart Cities* 2021;4:372–404. <https://doi.org/10.3390/smartcities4010022>.
- [3] Ambel CC, Earl T, Kenny S, Cornelis S, Sihvonen J. Roadmap to climate-friendly land freight and buses in Europe. 2017.
- [4] Yan S, de Bruin K, Dennehy E, Curtis J. Climate policies for freight transport: Energy and emission projections through 2050. *Transp Policy* 2021;107. <https://doi.org/10.1016/j.tranpol.2021.04.005>.
- [5] Moultak M, Lutsey N, Hall D. Transitioning to zero-emission heavy-duty freight vehicles. *Int Counc Clean Transp* 2017.
- [6] Cooper KR. Truck aerodynamics reborn - Lessons from the past. *SAE Tech Pap* 2003. <https://doi.org/10.4271/2003-01-3376>.
- [7] Den Boer E, Aarnink S, Kleiner F, Pagenkopf J. Zero emissions trucks. An overview of state-of-the-art technologies and their potential 2013.
- [8] Skrucany T, Sarkan B, Gnap J. Influence of aerodynamic trailer devices on drag reduction measured in a wind tunnel. *Ekspolatacja i Niezawodn - Maint Reliab* 2016;18:151–4. <https://doi.org/10.17531/ein.2016.1.20>.
- [9] Hariram A, Koch T, Mårdberg B, Kyncl J. A study in options to improve aerodynamic profile of heavy-duty vehicles in Europe. *Sustain* 2019;11:5519. <https://doi.org/10.3390/su11195519>.
- [10] Hjelm L, Bergqvist B. European truck aerodynamics - A comparison between conventional and CoE truck aerodynamics and a look into future trends and possibilities. *Lect. Notes Appl. Comput. Mech.*, vol. 41, 2009, p. 469–77. [https://doi.org/10.1007/978-3-540-85070-0\\_45](https://doi.org/10.1007/978-3-540-85070-0_45).
- [11] Hyams DG, Sreenivas K, Pankajakshan R, Stephen Nichols D, Roger Briley W, Whitfield DL. Computational simulation of model and full scale Class 8 trucks with drag reduction devices. *Comput Fluids* 2011;41:27–40. <https://doi.org/10.1016/j.compfluid.2010.09.015>.
- [12] Humphreys L, Bevely D. Computational Fluid Dynamic Analysis of a Generic 2 Truck Platoon. *SAE Tech. Pap.*, vol. 2016- Octob, 2016. <https://doi.org/10.4271/2016-01-8008>.
- [13] Khosravi M, Osaddeghi F, Veisi M, Hodayari-b A. Aerodynamic drag reduction of heavy vehicles using append devices by CFD analysis. *J Cent South Univ* 2015;22:4645–52. <https://doi.org/10.1007/s11771-015-3015-7>.
- [14] Miralbes R, Castejon L. Aerodynamic analysis of some boat tails for heavy vehicles. *Int J Heavy Veh Syst* 2012;19:115–27. <https://doi.org/10.1504/IJHVS.2012.046830>.
- [15] Mohamed-Kassim Z, Filippone A. Fuel savings on a heavy vehicle via aerodynamic drag reduction. *Transp Res Part D Transp Environ* 2010;15:275–84. <https://doi.org/10.1016/j.trd.2010.02.010>.
- [16] Selenbas B, Gunes H, Gocmen K, Bahceci U, Bayram B. An aerodynamic design and optimization of a heavy truck for drag reduction. *ASME 2010 10th Bienn. Conf. Eng. Syst. Des. Anal. ESDA2010*, vol. 3, 2010, p. 121–9. <https://doi.org/10.1115/ESDA2010-24482>.
- [17] Graichen J. Targets for the non-ETS sectors in 2040 and 2050. *Öko-Institut EV* 2016.
- [18] Earl T, Mathieu L, Cornelis S, Kenny S, Ambel CC, Nix J. Analysis of long haul battery electric trucks in EU. *8th Commer Veh Work* 2018.

- [19] Kouchak SM, Gaffar A. Determinism in future cars: why autonomous trucks are easier to design. 2017 IEEE SmartWorld, Ubiquitous Intell. Comput. Adv. Trust. Comput. Scalable Comput. Commun. Cloud Big Data Comput. Internet People Smart City Innov., IEEE; 2017, p. 1–6. <https://doi.org/10.1109/UIC-ATC.2017.8397598>.
- [20] World Health Organization. 2018. Global status report on road safety 2018. [Online] Available at: <https://www.who.int/publications/i/item/9789241565684> [Accessed 30 May 2021] n.d.
- [21] Mobility and Transport. Intelligent transport systems. [Online] Available at: [https://ec.europa.eu/transport/themes/its/road\\_it](https://ec.europa.eu/transport/themes/its/road_it) [Accessed 30 May 2021]. n.d.
- [22] Verster T, Fourie E. The good, the bad and the ugly of South African fatal road accidents. S Afr J Sci 2018;114. <https://doi.org/10.17159/sajs.2018/20170427>.
- [23] Singh S. Critical reasons for crashes investigated in the National Motor Vehicle Crash Causation Survey. Natl Highw Traffic Saf Adm 2015.
- [24] “Intelligent transport systems.” Road | Mobility and Transport n.d.
- [25] Arora S, Abkenar AT, Jayasinghe SG, Tammi K. Heavy-duty Electric Vehicles: From Concept to Reality. Butterworth-Heinemann; 2021.
- [26] Verbruggen FJR, Silvas E, Hofman T. Electric powertrain topology analysis and design for heavy-duty trucks. Energies 2020;13:2434. <https://doi.org/10.3390/en13102434>.
- [27] Mareev I, Becker J, Sauer DU. Battery dimensioning and life cycle costs analysis for a heavy-duty truck considering the requirements of long-haul transportation. Energies 2018;11:55. <https://doi.org/10.3390/en11010055>.
- [28] Morozov A, Humphries K, Zou T, Rahman T, Angeles J. Design, Analysis, and Optimization of a Multi-Speed Powertrain for Class-7 Electric Trucks. SAE Int J Altern Powertrains 2018;7. <https://doi.org/10.4271/08-07-01-0002>.
- [29] Wolff S, Kalt S, Bstiel M, Lienkamp M. Influence of powertrain topology and electric machine design on efficiency of battery electric trucks—a simulative case-study. Energies 2021;14:328. <https://doi.org/10.3390/en14020328>.
- [30] Storms BL, Satran DR, Heineck JT, Walker SM. A summary of the experimental results for a generic tractor-trailer in the ames research center 7-by 10-foot and 12-foot wind tunnels 2006.
- [31] Satran D. An experimental study of the generic conventional model (gcm) in the nasa ames 7-by-10-foot wind tunnel. Aerodyn. Heavy Veh. Truck. Buses, Trains, Springer; 2004, p. 171–171. [https://doi.org/10.1007/978-3-540-44419-0\\_18](https://doi.org/10.1007/978-3-540-44419-0_18).
- [32] Lanfrit, M. 2005. A best practice guideline to handle Automotive External Aerodynamics with FLUENT. Fluent Inc. Technical Notes. [Online] Available at: [https://www.southampton.ac.uk/~nwb/lectures/GoodPracticeCFD/Articles/Ext\\_Aero\\_Best\\_Practice\\_Ver1\\_2.pdf](https://www.southampton.ac.uk/~nwb/lectures/GoodPracticeCFD/Articles/Ext_Aero_Best_Practice_Ver1_2.pdf) n.d.
- [33] Versteeg HK, Malalasekera W. An Introduction to the fluid dynamics - The Finite Volume Method. 2nd ed. Harlow: Pearson Education Limited 2007.
- [34] Anderson Jr JD. Fundamentals of aerodynamics. 5th ed. McGraw-Hill Education; 2010.
- [35] Katz J. Automotive aerodynamics. 1st ed. John Wiley & Sons; 2016.
- [36] Wendt JF. Computational fluid dynamics: an introduction. 3rd ed. Springer Science & Business Media; 2008.
- [37] Nunn RH. Intermediate fluid mechanics. 1st ed. Routledge; 2018. <https://doi.org/10.1201/9780203750384>.
- [38] Ansys. Ansys Fluent 12.0 Theory Guide - 18.4.3 Pressure-Velocity Coupling 2009.